Enhanced Visible-Light-Driven Photodegradation of Rhodamine B over $Ag_2C_2O_4/Bi_2MoO_6$ Nanocomposites

Phuruanqrat, Anukorn*[+]; Junsang, Chanisara
Division of Physical Science, Faculty of Science, Prince of Songkla University, Hat Yai, Songkhla 90112, THAILAND

Patiphatpanya, Panudda; Dumrongrojthanath, Phattranit
Department of Chemistry, Faculty of Science, Chiang Mai University, Chiang Mai 50200, THAILAND

Ekthammathat, Nuengruethai
Program in Chemistry, Faculty of Science and Technology, Bansomdejchaopraya Rajabhat University, Bangkok 10600, THAILAND

Karthik, Astro
School of Physics, Bharathidasan University, Tiruchirappalli - 620 024, Tamil Nadu, INDIA

***Thongtem, Somchai*[•]**
Department of Physics and Materials Science, Faculty of Science, Chiang Mai University, Chiang Mai 50200, THAILAND

Thongtem, Titipun*[•]
Department of Chemistry, Faculty of Science, Chiang Mai University, Chiang Mai 50200, THAILAND

ABSTRACT: *In the present work, $Ag_2C_2O_4/Bi_2MoO_6$ nanocomposites containing different weight contents of $Ag_2C_2O_4$ were prepared by a deposition-precipitation method. The products were characterized by X-ray diffraction (XRD), scanning electron microscopy (SEM), transmission electron microscopy (TEM), high-resolution transmission electron microscopy (HRTEM), and selected area electron diffraction (SAED). They revealed the presence of good crystalline monoclinic $Ag_2C_2O_4$ nanoparticles distributed on orthorhombic Bi_2MoO_6 square nanoplates. The photocatalytic properties of Bi_2MoO_6 and $Ag_2C_2O_4/Bi_2MoO_6$ samples were investigated by photodegradation of rhodamine B (RhB) under visible light irradiation. In this research, 10 wt% $Ag_2C_2O_4/Bi_2MoO_6$ nanocomposites have the highest photocatalytic performance of 78.84 % within 100 min under visible light irradiation, higher than the photocatalytic performance of pure Bi_2MoO_6. A photocatalytic mechanism of $Ag_2C_2O_4/Bi_2MoO_6$ nanocomposites was also discussed according to the experimental results.*

KEYWORDS: *Heterostructure nanocomposites; Photocatalysis; Spectroscopy; Electron microscopy*

* *To whom correspondence should be addressed.*
+ E-mail: phuruangrat@hotmail.com ; ttpthongtem@yahoo.com
• Other Address: Materials Science Research Center, Faculty of Science, Chiang Mai University, Chiang Mai 50200, THAILAND
1021-9986/2020/4/29-37 9/$/5.09

INTRODUCTION

Over a period of ten years, advanced oxidation process (AOP) has been actively developed because environmental treatment for human health deals with heavy discharge of wastewater and organic dyes of industries in order to attain completely degradable, clean and renewable features [1–3]. TiO_2 has been proved to be the most effective photocatalyst used for decomposition of numerous compounds. A relatively wide band gap of ~3.2 eV for anatase or 3.0 eV for rutile prohibits the photocatalytic reaction because only ultraviolet fraction in solar light (< 3–5%) is absorbed [4, 5]. Thus the development of visible light induced photocatalyst is of great importance for efficient utilization of solar energy for photocatalytic degradation of organic pollutants and splitting of water.

Recently, bismuth-based materials such as BiOX (X = Cl, Br, I) [4, 6], $BiVO_4$ [7, 8], Bi_2WO_6 [1–3] and Bi_2MoO_6 [5, 9, 10–12] show promising application for photocatalysis of organic pollutant induced by visible radiation due to their unique crystalline structure, energy band structure, chemical stability, nontoxicity and relatively high photocatalytic activity for removal of organic pollutants [6, 7, 13]. Among oxide-based semiconductors, a naturally abundant, high quantum yield and non-toxic Bi_2MoO_6 material has promising candidate dielectric, ion-conductive, luminescent and catalytic properties [5, 9]. Furthermore, Bi_2MoO_6 has a unique layered structure constructed by alternate stacking of corner-shared and distorted MoO_6 octahedron and bismuth oxide $[Bi_2O_2]^{2+}$ layers [9, 11, 12]. It is an excellent photocatalyst for degradation of organic compounds under visible-light irradiation such as methylene blue [5, 14], rhodamine B [10, 14], methyl orange [11], tetracycline [12] and phenol [15, 16]. Moreover, the photocatalytic performance of Bi_2MoO_6 is limited by rapid recombination of electron-hole pairs [9, 11, 14, 15]. To succeed in dealing with this problem, further study is in urgent need to improve its photocatalytic properties.

Construction of heterojunction photocatalyst is generally known to be an effective method to promote the separation of photoexcited electron-hole pairs and to enhance the photocatalytic performance [1, 2, 7]. Ag-based photocatalyst mixed with other semiconductor photocatalyst was used to improve photocatalytic activity owing to the narrow band gap energy and strong visible light absorption [17, 18]. Feng at al. reported that $Ag_2C_2O_4/TiO_2$ nanocomposites showed much higher photocatalytic activity for degradation of propylene and acetaldehyde gas under visible light irradiation than pure $Ag_2C_2O_4$ and P25-TiO_2 [18]. *Xiang et al.* claimed that Ag_2CO_3 deposited on the surface of ZnO by precipitation method can lead to improve the separation of photo-induced charge carrier of ZnO and show excellent photocatalytic reaction of RhB under visible light irradiation [19].

In this present research, $Ag_2C_2O_4/Bi_2MoO_6$ heterostructure nanocomposites with different weight contents of $Ag_2C_2O_4$ were prepared by a deposition-precipitation method. The products were characterized by XRD, SEM TEM, HRTEM and SAED. Their photocatalytic performance was investigated by photodegradation of rhodamine B (RhB) under visible light irradiation. The photocatalytic mechanism of $Ag_2C_2O_4/Bi_2MoO_6$ was also discussed according to the experimental results.

EXPERIMENTAL SECTION

The Bi_2MoO_6 nanoplates were synthesized by a hydrothermal method. Bismuth nitrate hexahydrate ($Bi(NO_3)_3{\cdot}6H_2O$, Loba Chemie Pvt. Ltd., India) and sodium molybdate dihydrate ($Na_2MoO_4{\cdot}2H_2O$, Loba Chemie Pvt. Ltd., India) were analytical grade and used without further purification. In a typical synthesis, 0.005 mole $Na_2MoO_4{\cdot}2H_2O$ was dissolved in 100 ml reverse osmosis (RO) water with continuous stirring at room temperature for 30 min, and followed by 0.01 mole $Bi(NO_3)_3{\cdot}6H_2O$ adding. The final mixture was stirred for at least 30 min. Subsequently, 3 M NaOH was added to the mixture until achieving at the desired pH of 10. The solution mixture was transferred to a 200 ml Teflon-lined autoclave and heated to 180 °C for 20 h. The resulting suspension was left to naturally cool down to room temperature. Following the centrifugation, the obtained white precipitates were washed with absolute ethanol and distilled water several times and dried in an oven at 60 °C for 12 h.

To synthesize $Ag_2C_2O_4$ nanoparticles with different contents deposited on Bi_2MoO_6 nanoplates, different concentrations of 0–10 % $AgNO_3$ and Na_2CO_3 by weight and 1 g Bi_2MoO_6 sample were dissolved in 100 ml RO

water under magnetic stirring for 24 h. Then the products were separated by filtering, washed by absolute ethanol and dried at 80 °C in an electric oven for 24 h.

XRD patterns of the products were recorded on a Philips X'Pert MPD X-ray diffractometer equipped with Cu K_α radiation ranging from 10° to 80° at a scanning rate of 0.02 deg/s. SEM and TEM images were taken by a scanning electron microscope, JEOL JSM 6335F with an acceleration voltage of 20 kV and a transmission electron microscope, JEOL JEM 2010 with an acceleration voltage of 200 kV.

The photocatalytic activities of as-synthesized samples were evaluated via photodegradation of RhB solution under visible light irradiation of Xe lamp as a light source. A 200 mg photocatalyst was suspended in a 200 ml 10^{-5} M RhB solution each. The suspension was stirred in the dark for 30 min to establish an adsorption-desorption equilibrium of RhB and photocatalyst. Then the solutions were irradiated by visible light of Xe lamp at room temperature for different lengths of time. The RhB concentration was measured by a UV-visible spectrophotometer (Lambda 25 spectrometer, Perkin Elmer) at λ_{max} of RhB = 554 nm. The decolorization efficiency was calculated by the following equation.

$$\text{Decolorization efficiency (\%)} = \frac{C_o - C_t}{C_o} \times 100 \qquad (1)$$

where C_o is the initial concentration of RhB and C_t is the concentration of RhB after light irradiation for a period of time (t).

RESULTS AND DISCUSSION

Fig. 1 shows XRD patterns the 0–10 wt% $Ag_2C_2O_4/Bi_2MoO_6$ heterostructure over 2θ of 10°–80° which revealed the phase of Bi_2MoO_6 sample and $Ag_2C_2O_4/Bi_2MoO_6$ heterostructure composites. It can be seen that the pure Bi_2MoO_6 sample shows prominent diffraction peaks which were indexed to pure orthorhombic Bi_2MoO_6 phase as compared with the JCPDS No. 21-0102 [20]. Impurities such as Bi_2O_3, MoO_3, etc were not detected, showing that the as-synthesized Bi_2MoO_6 phase is highly pure. Upon adding different weight contents of $Ag_2C_2O_4$, the additional characteristic monoclinic $Ag_2C_2O_4$ phase (JCPDS No. 04-0660 [20]) were detected in $Ag_2C_2O_4/Bi_2MoO_6$ heterostructure composites. Comparing to Bi_2MoO_6, XRD peaks of $Ag_2C_2O_4/Bi_2MoO_6$ heterostructure were

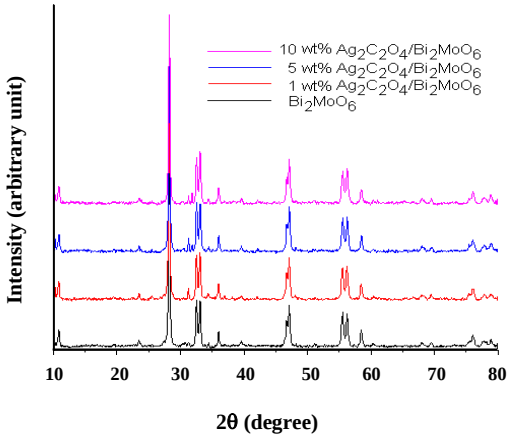

Fig. 1: XRD patterns of 0–10 wt% $Ag_2C_2O_4/Bi_2MoO_6$ samples.

still in the same position as those of Bi_2MoO_6, suggesting that the loaded $Ag_2C_2O_4$ did not change the bulk intrinsic property of the Bi_2MoO_6 sample. Therefore, the XRD results certified the formation of high purified monoclinic $Ag_2C_2O_4$ nanoparticles supported on the orthorhombic Bi_2MoO_6 surface by forming $Ag_2C_2O_4/Bi_2MoO_6$ heterostructure composites.

The morphologies of pure Bi_2MoO_6 sample and $Ag_2C_2O_4/Bi_2MoO_6$ composites were observed by SEM as the results shown in Fig. 2. SEM image of pure Bi_2MoO_6 appears as uniform square nanoplates with edge length of 500–800 nm and thickness of 20 nm and a relatively narrow grain size distribution. The surface of Bi_2MoO_6 nanoplates was very smooth. For the $Ag_2C_2O_4/Bi_2MoO_6$ heterostructure images, they were still nanoplates, indicating that the loaded $Ag_2C_2O_4$ did not alter the morphology of Bi_2MoO_6. Moreover, the good dispersive and uniform spherical $Ag_2C_2O_4$ nanoparticles with the diameter of < 100 nm supported on the surface of Bi_2MoO_6 nanoplates were detected on the $Ag_2C_2O_4/Bi_2MoO_6$ heterostructure nanocomposites, implying that $Ag_2C_2O_4$ nanoparticles were successfully deposited on the surface of Bi_2MoO_6 nanoplates. The uniform size of the $Ag_2C_2O_4$ nanoparticles deposited on the Bi_2MoO_6 surface was detected. Due to the limited number of reaction sites on Bi_2MoO_6, the growth and the aggregation of $Ag_2C_2O_4$ nanoparticles were prohibited and the pre-adsorption of Ag^+ played the role in prohibiting the growth of $Ag_2C_2O_4$ nanoparticles [21]. Moreover, the EDS analysis indicated that the 10 wt% $Ag_2C_2O_4/Bi_2MoO_6$ nanocomposites were composed of Ag, C, Bi, Mo and O elements, certifying

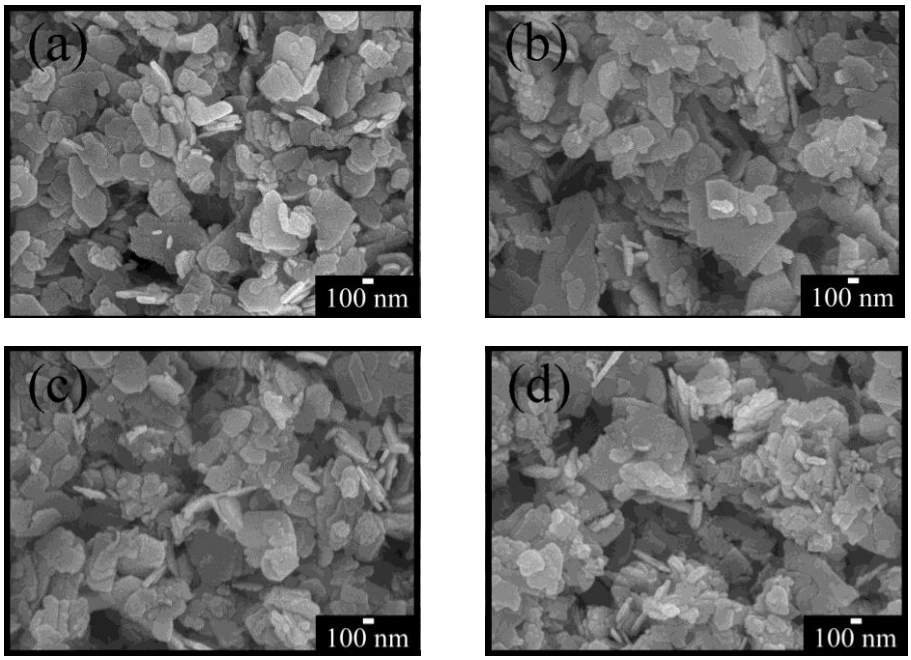

Fig. 2: SEM images of (a) pure Bi_2WO_6, (b) 1 wt% $Ag_2C_2O_4/Bi_2MoO_6$, (c) 5 wt% $Ag_2C_2O_4/Bi_2MoO_6$ and (d) 10 wt% $Ag_2C_2O_4/Bi_2MoO_6$ samples.

that the as-obtained nanocomposites were the $Ag_2C_2O_4$ and Bi_2MoO_6 combination.

Fig. 3 shows the TEM, SAED and HRTEM results of Bi_2MoO_6, 5 wt% $Ag_2C_2O_4/Bi_2MoO_6$ and 10 wt% $Ag_2C_2O_4/Bi_2MoO_6$. The TEM image of Bi_2MoO_6 sample shows nanoplates with edge length of 50–200 nm. Its SAED pattern shows well-defined bright spots of electron diffraction revealing good single crystalline Bi_2MoO_6 phase. The SAED pattern was indexed to the (060), (062) and (002) planes of orthorhombic Bi_2MoO_6 phase with zone axis of [100]. This shows that the (100) surface is preferential orientation of orthorhombic Bi_2MoO_6 structure. TEM images of 5 wt% and 10 wt% $Ag_2C_2O_4/Bi_2MoO_6$ nanocomposites showed uniformly distributed nanoparticles on the surface of Bi_2MoO_6 nanoplates. The average particles are 5–20 nm in size. With the increment increase of $Ag_2C_2O_4$ content to 10 wt%, more $Ag_2C_2O_4$ nanoparticles were fully deposited and randomly dispersed on the surface of Bi_2MoO_6. TEM image of typical 10 wt% $Ag_2C_2O_4/Bi_2MoO_6$ nanocomposites at high magnification shows truly spherical $Ag_2C_2O_4$ nanoparticles with less than 10 nm. The HRTEM image of typical 10 wt% $Ag_2C_2O_4/Bi_2MoO_6$ nanocomposites clearly shows interface of junction between $Ag_2C_2O_4$ and Bi_2MoO_6 attributed to the separation of photo-excited charge carriers [7, 13]. A lattice space of 0.285 nm corresponds with the (110) crystalline plane of $Ag_2C_2O_4$ phase.

The photocatalytic activity of the pure Bi_2MoO_6 and $Ag_2C_2O_4/Bi_2MoO_6$ samples was monitored through photodegradation of RhB under visible light irradiation ($\lambda \geq 420$ nm). Fig. 4 shows UV-visible spectra of temporal evolution for photodegradation of RhB under visible light irradiation within 100 min by Bi_2MoO_6 and 10 wt% $Ag_2C_2O_4/Bi_2MoO_6$ photocatalysts. They can be seen that the absorption intensity of RhB spectra decreases with the increase of exposure time of visible light irradiation. The RhB solution photodegraded by Bi_2MoO_6 remains as pink color while that photodegraded by $Ag_2C_2O_4/Bi_2MoO_6$ was transformed into almost white under visible-light irradiation within 100 min. The 10 wt% $Ag_2C_2O_4/Bi_2MoO_6$ nanocomposites showed higher photocatalytic activity for decolorization of RhB aqueous solution than Bi_2MoO_6. At the end of 100 min visible light irradiation, the maximum absorption peak of RhB at 554 nm was shifted to a shorter wavelength of 498 nm,

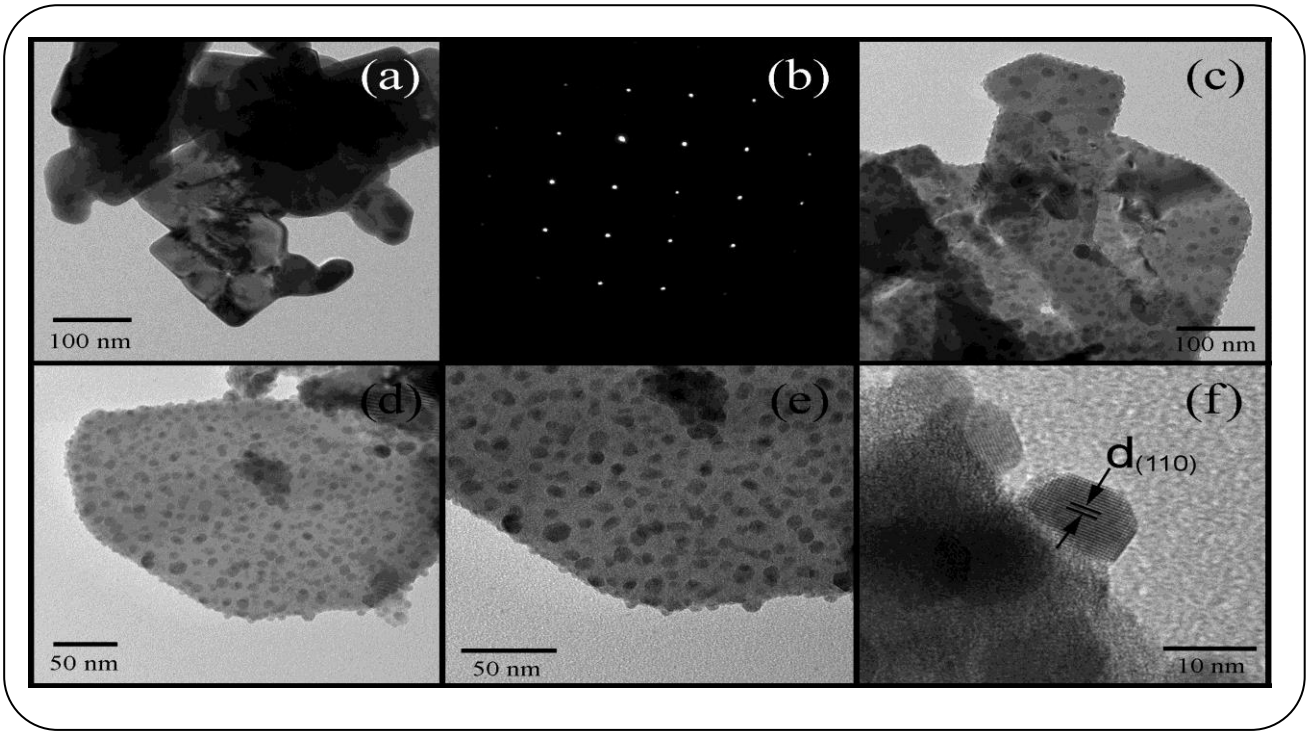

Fig. 3: TEM images, HRTEM images and SAED pattern of (a and b) pure Bi_2MoO_6, (c) 5 wt% $Ag_2C_2O_4/Bi_2MoO_6$ and (d–f) 10 wt% $Ag_2C_2O_4/Bi_2MoO_6$ samples.

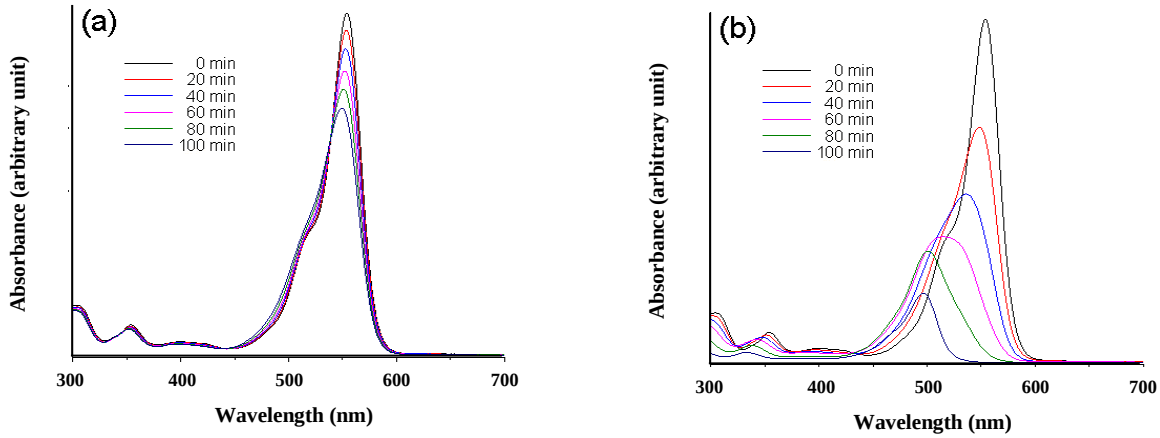

Fig. 4: UV-visible absorption of RhB after being photocatalyzed by (a) Bi_2MoO_6 sample and (b) 10 wt% $Ag_2C_2O_4/Bi_2MoO_6$ nanocomposites under visible light within 100 min.

attributed to the de-ethylation of RhB by active species during photocatalytic reaction [22–24].

Fig. 5a shows the relative concentration of RhB remaining in the solution as a function of irradiation time during the photocatalytic process by Bi_2MoO_6 and $Ag_2C_2O_4/Bi_2MoO_6$ samples under visible light irradiation. It can be seen that no obvious degradation of RhB was detected without photocatalyst. At the adsorption–desorption equilibrium between photocatalyst and RhB, the RhB molecules were adsorbed around 18–21 % for Bi_2MoO_6 and $Ag_2C_2O_4/Bi_2MoO_6$ samples. The pure Bi_2MoO_6 sample exhibited poor photodecolorization efficiency of 24.53 % after 100 min of visible light irradiation. But for all $Ag_2C_2O_4/Bi_2MoO_6$ heterostructure composites with different loaded $Ag_2C_2O_4$ contents showed higher photocatalytic activity than the pure

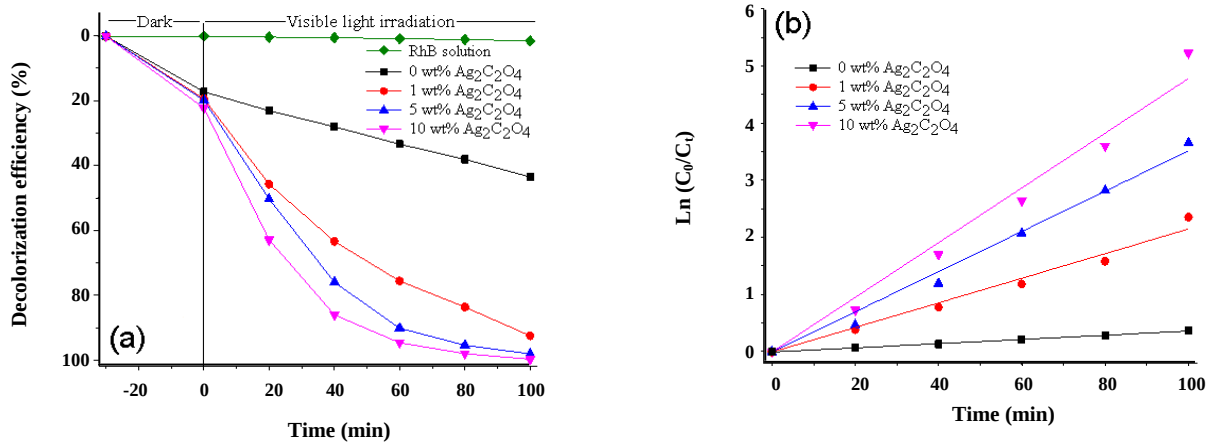

Fig. 5: (a) Decolorization efficiency and (b) first-order plot for photocatalytic degradation of RhB by 0–10 wt% $Ag_2C_2O_4/Bi_2MoO_6$ photocatalysts under visible light within 100 min.

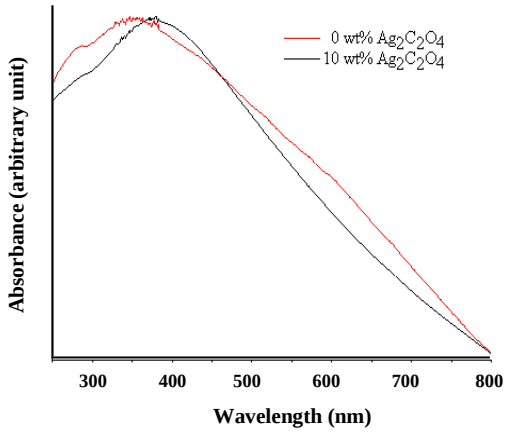

Fig. 6: UV-visible absorption of Bi_2MoO_6 and 10 wt% $Ag_2C_2O_4/Bi_2MoO_6$ samples.

Bi_2MoO_6 sample. These results were ascribed to the lowest rate of photoinduced electron-hole recombination and the good absorption in visible light as the results shown in Fig. 6. Fig. 6 shows the UV-visible absorption spectra of Bi_2MoO_6 and 10 wt% $Ag_2C_2O_4/Bi_2MoO_6$ samples in wavelength of 200–800 nm. Good UV-visible absorption was observed because the electronic transition from valence band to conduction band. Moreover, 10 wt% $Ag_2C_2O_4/Bi_2MoO_6$ showed higher UV-visible absorption than pure Bi_2MoO_6, indicating that more photoinduced electron-hole pairs were produced and were able to accelerate the photocatalytic activity for RhB degradation by 10 wt% $Ag_2C_2O_4/Bi_2MoO_6$ photocatalyst. The photodegradation efficiencies of RhB in the presence of different photocatalysts under visible light within 100 min were 70.93, 76.74 and 78.84 % for 1 wt% $Ag_2C_2O_4/Bi_2MoO_6$, 5 wt% $Ag_2C_2O_4/Bi_2MoO_6$ and 10 wt% $Ag_2C_2O_4/Bi_2MoO_6$, respectively. The 10 wt% $Ag_2C_2O_4/Bi_2MoO_6$ nanocomposites exhibited higher photocatalytic activity than other photocatalysts.

According to the previous reports, the degradation of dyes can be ascribed to a pseudo-first-order reaction based on the Langmuir–Hinshelwood model for fitting empirical data through the following equation

$$\ln\frac{C_o}{C_t} = kt \qquad (2)$$

where k is the apparent pseudo-first-order rate constant (min^{-1}), C_o is the initial RhB concentration and C_t is the RhB concentration in an aqueous solution within a period of irradiation time [25, 26]. Fig. 5b shows the photocatalytic degradation of RhB as a function of irradiation time (t). The plot of $\ln C_o/C_t$ vs t shows a linear relationship which certified that the photodegradation of RhB followed the first-order kinetics. The 10 wt% $Ag_2C_2O_4/Bi_2MoO_6$ nanocomposites have the highest rate constant (0.0477 min^{-1}) which is 12 times of that of Bi_2MoO_6 (0.0040 min^{-1}). The results indicated that the deposition of $Ag_2C_2O_4$ nanoparticles on the surface of Bi_2MoO_6 nanoplates was favorable for the diffusion of photoinduced electrons and holes, resulting in improving photocatalytic activity of $Ag_2C_2O_4/Bi_2MoO_6$ nanocomposites [27].

The photocatalytic activity of $Ag_2C_2O_4/Bi_2MoO_6$ nanocomposites was higher than that of Bi_2MoO_6. Possibly, there might have synergic effect between

$Ag_2C_2O_4$ and Bi_2MoO_6. This effect was attributed to efficient charge diffusion across the composites. It was able to prohibit photoexcited electron–hole recombination and to enhance photocatalytic performance [28–30]. An appropriate band potential is a parameter to determine the synergic effect. Both Bi_2MoO_6 and $Ag_2C_2O_4$ could absorb visible light and were all excited to generate electron–hole pairs at conduction and valance bands. Subsequently, photoinduced electrons and holes diffused across the $Ag_2C_2O_4$–Bi_2MoO_6 interface resulting to prevent the recombination process and improve the photodegradation reaction. Then, the photoinduced electrons and holes can react with surface-adsorbed O_2 and OH^- on the $Ag_2C_2O_4$ active sites to generate $^{\bullet}O_2^-$ and $^{\bullet}OH$ radicals which further oxidized RhB molecules to form CO_2 and water. Thus it is reasonable to claim that the $Ag_2C_2O_4/Bi_2MoO_6$ nanocomposites exhibit higher photocatalytic activity than pure Bi_2MoO_6.

CONCLUSIONS

Heterostructure $Ag_2C_2O_4/Bi_2MoO_6$ nanocomposites were successfully synthesized by a deposition-precipitation method. The analytical results show good distribution of $Ag_2C_2O_4$ nanoparticles supported on Bi_2MoO_6 nanoplates. The 10 wt% $Ag_2C_2O_4/Bi_2MoO_6$ nanocomposites showed the highest photocatalytic activity for degradation of RhB under visible light irradiation.

Acknowledgments

We are extremely grateful to Prince of Songkla University, Hat Yai, Songkhla 90112, Thailand for providing financial support through the contact no. SCI610022S, and Center of Excellence in Materials Science and Technology, Chiang Mai University under the administration of Materials Science Research Center, Faculty of Science, Chiang Mai University, Thailand.

Received : Dec. 16, 2018 ; Accepted :Apr. 15, 2019

REFERENCES

[1] Wang G., Wang L., Hydrothermal Synthesis of Rose-Like $AgVO_3/Bi_2WO_6$ Heterojunctions with Enhanced Visible-Light-Driven Photocatalytic Activity, *Physica E*, **103**: 323–328 (2018).

[2] Long G., Ding J., Xie L., Sun R., Chen M., Zhou Y., Huang X., Han G., Li Y., Zhao W., Fabrication of Mediator-Free g-C_3N_4/Bi_2WO_6 Z-Scheme with Enhanced Photocatalytic Reduction Dechlorination Performance of 2,4-DCP, *Appl. Surf. Sci.*, **455**: 1010–1018 (2018).

[3] Zhang S., Pu W., Du H., Wang Y., Yang C., Gong J., Facile Synthesis of Pt Assisted Bi-Bi_2WO_{6-x} with Oxygen Vacancies for the Improved Photocatalytic Activity under Visible Light, *Appl. Surf. Sci.*, **459**: 363–375 (2018).

[4] Shenawi-Khalil S., Uvarov V., Menes E., Popov I., Sasson Y., New Efficient Visible Light Photocatalyst Based on Heterojunction of BiOCl–Bismuth Oxyhydrate, *Appl. Catal. A*, **413–414**: 1–9 (2012).

[5] Guo J., Shi L., Zhao J., Wang Y., Tang K., Zhang W., Xie C., Yuan X., Enhanced Visible-Light Photocatalytic Activity of Bi_2MoO_6 Nanoplates with Heterogeneous Bi_2MoO_6-x@Bi_2MoO_6 Core-Shell Structure, *Appl. Catal. B*, **224**: 692–704 (2018).

[6] Xiao X., Zheng C., Lu M., Zhang L., Liu F., Zuo X., Nan J., Deficient $Bi_{24}O_{31}Br_{10}$ as a Highly Efficient Photocatalyst for Selective Oxidation of Benzyl Alcohol into Benzaldehyde under Blue LED Irradiation, *Appl. Catal. B*, **228**: 142–151 (2018).

[7] Liu Y., Kong J., Yuan J., Zhao W., Zhu X., Sun C., Xie J., Enhanced Photocatalytic Activity over Flower-Like Sphere $Ag/Ag_2CO_3/BiVO_4$ Plasmonic Heterojunction Photocatalyst for Tetracycline Degradation, *Chem. Eng. J.*, **331**: 242–254 (2018).

[8] Shi Y., Hu Y., Zhang L., Yang Z., Zhang Q., Cui H., Zhu X., Wang J., Chen J., Wang K., Palygorskite Supported $BiVO_4$ Photocatalyst for Tetracycline Hydrochloride Removal, *Appl. Clay Sci.*, **137**: 249–258 (2017).

[9] Zhang B., Li J., Gao Y., Chong R., Wang Z., Guo L., Zhang X., Li C., To Boost Photocatalytic Activity in Selective Oxidation of Alcohols on Ultrathin Bi_2MoO_6 Nanoplates with Pt Nanoparticles as Cocatalyst, *J. Catal.*, **345**: 96–103 (2017).

[10] Wang Q., Sun K., Lu Q., Wei M., Yao L., Guo E., Synthesis of Novel Elm Branch-Like Hierarchical γ-Bi_2MoO_6 Nanostructures with Enhanced Visible-Light-driven Photocatalytic Performance, *Dyes Pigments*, **155**: 194–201 (2018).

[11] Geng B., Wei B., Gao H., Xu L., Ag_2O Nanoparticles Decorated Hierarchical Bi_2MoO_6 Microspheres for Efficient Visible Light Photocatalysts, *J. Alloy. Compd.*, **699**: 783–787 (2017).

[12] Bai J., Li Y., Liu J., Liu L., 3D Bi_2MoO_6 Hollow Mesoporous Nanostructures with High Photodegradation for Tetracycline, *Microporous. Mesoporous. Mater.*, **240**: 91–95 (2017).

[13] Li T., Hu X., Liu C., Tang C., Wang X., Luo S., Efficient Photocatalytic Degradation of Organic dyes and Reaction Mechanism with $Ag_2CO_3/Bi_2O_2CO_3$ Photocatalyst under Visible Light Irradiation, *J. Mole. Catal. A*, **425**: 124–135 (2016).

[14] Sun C., Xu Q., Xie Y., Ling Y., Jiao J., Zhu H., Zhao J., Liu X., Hu B., Zhou D., High-Efficient One-Pot Synthesis of Carbon Quantum Dots Decorating Bi2MoO6 Nanosheets Heterostructure with Enhanced Visible-Light Photocatalytic Properties, *J. Alloy. Compd.*, **723**: 333–344 (2017).

[15] Meng X., Zhang Z., Pd-doped Bi_2MoO_6 Plasmonic Photocatalysts with Enhanced Visible Light Photocatalytic Performance, *Appl. Surf. Sci.*, **392**: 169–180 (2017).

[16] Yin W., Wang W., Sun S., Photocatalytic Degradation of Phenol over Cage-Like Bi_2MoO_6 Hollow Spheres under Visible-Light Irradiation, Catal. Commun., **11**: 647–650 (2010).

[17] Li J., Fang W., Yu C., Zhou W., Zhu L., Xie Y., Ag-Based Semiconductor Photocatalysts in Environmental Purification, *Appl. Surf. Sci.*, **358**: 46–56 (2015).

[18] Feng C., Sun M., Wang Y., Huang X., Zhang A., Pang Y., Zhou Y., Peng L., Ding Y., Zhang L., Li D., $Ag_2C_2O_4$ and $Ag_2C_2O_4/TiO_2$ Nanocompositesas Highly Efficient and Stable Photocatalyst under Visible Light: Preparation, Characterization and Photocatalytic Mechanism, *Appl. Catal. B*, **219**: 705–714 (2017).

[19] Xiang Z., Zhong J., Huang S., Li J., Chen J., Wang T., Li M., Wang P., Efficient Charge Separation of Ag_2CO_3/ZnO Composites Prepared by a Facile Precipitation Approach and its Dependence on Loading Content of Ag_2CO_3, *Mater. Sci. Semicond. Process.*, **52**: 62–67 (2016).

[20] Powder Diffract. File, JCPDS-ICDD, 12 Campus Boulevard, Newtown Square, PA 19073-3273, U.S.A., (2001).

[21] Wang P., Li Y., Liu Z., Chen J., Wu Y., Guo M., Na P., In-Situ Deposition of Ag_3PO_4 on TiO_2 Nanosheets Dominated by (001) Facets for Enhanced Photocatalytic Activities and Recyclability, *Ceram. Inter.*, **43**: 11588–11595 (2017).

[22] Hu Y., Li D., Wang H., Zeng G., Li X., Shao Y., Role of Active Oxygen Species in the Liquid-Phase Photocatalytic Degradation of RhB Using $BiVO_4/TiO_2$ Heterostructure under Visible Light Irradiation, *J. Mole. Catal. A*, **408**: 172–178 (2015).

[23] Hu L., Deng G., Lu W., Pang S., Hu X., Deposition of CdS Nanoparticles on MIL-53(Fe) Metal-Organic Framework with Enhanced Photocatalytic Degradation of RhB under Visible Light Irradiation, Appl. Surf. Sci., **410**: 401–413 (2017).

[24] Ge S., Wang B., Li D., Fa W., Yang Z., Yang Z., Jia G., Zheng Z., Surface Controlled Photocatalytic Degradation of RhB over Flower-Like Rutile TiO_2 Superstructures, *Appl. Surf. Sci.*, **295**: 123–129 (2014).

[25] Intaphong P., Phuruangrat A., Thongtem S., Thongtem T., Sonochemical Synthesis and Characterization of BiOI Nanoplates for Using as Visible-Light-Driven Photocatalyst, *Mater. Lett.*, **213**: 88–91 (2018).

[26] Phuruangrat A., Thongtem S., Thongtem T., Microwave-Assisted Hydrothermal Synthesis and Characterization of CeO_2 Nanowires for Using as a Photocatalytic Material, *Mater. Lett.*, **196**: 61–63 (2017).

[27] Liu L., Luo X., Li Y., Xu F., Gao Z., Zhang X., Song Y., Xu H., Li H., Facile Synthesis of Few-Layer g-C_3N_4/ZnO Composite photocatalyst for Enhancing Visible Light Photocatalytic Performance of Pollutants Removal, *Colloid. Surf. A*, **537**: 516–523 (2018).

[28] Singh A., Sinha A.S.K., Active CdS/rGO photocatalyst by a High-Temperature Gas-Solid Reaction for Hydrogen Production by Splitting of Water, *Appl. Surf. Sci.*, **430**: 184–197 (2018).

[29] Wu K., Cui Y., Wei X., Song X., Huang J., The hybridization of Ag_2CO_3 Rods with g-C_3N_4 sheets with Improved Photocatalytic Activity, *J. Saudi Chem. Soc.*, **19**: 465–470 (2015).

[30] Kaur J., Gupta K., Kumar V., Bansal S., Singh S., Synergic Effect of Ag Decoration onto ZnO Nanoparticles for the Remediation of Synthetic Dye Wastewater, *Ceram. Inter.*, **42**: 2378–2385 (2016).